ELSEVIER

Coordination Chemistry Reviews
187 (1999) 151–181

COORDINATION CHEMISTRY REVIEWS

Water exchange on metal ions: experiments and simulations

L. Helm, A.E. Merbach *

Institut de Chimie Minérale et Analytique, Université de Lausanne, BCH, CH-1015 Lausanne, Switzerland

Received 18 August 1998; accepted 16 October 1998

Contents

Abstract

The water exchange reaction between coordination shells around metal ions in aqueous solution is a fundamental reaction in understanding the reactivity of these ions in chemical and biological systems. The results reviewed in this paper demonstrate the complementary of experimental studies and computer simulations or quantum chemical calculations performed on such systems. Due to the large range of exchange rate constants, a variety of experimental and different computer techniques have to be applied. Very fast exchange reactions between first and second coordination shell and between second shell and bulk solvent can be simulated by classical molecular dynamics technique. Reaction pathways for water exchange on metal ions with a less labile first coordination shell can be followed by calculation of

* Corresponding author. Tel.: +41-21-6923871; fax: +41-21-6923875.
E-mail address: andre.merbach@icma.unil.ch (A.E. Merbach)

PII: S0010-8545(99)00232-X

clearly defined transition states. Success and shortcomings of the techniques are discussed by means of recent publications.

Keywords: Water exchange reaction; Coordination shell; Reaction pathways

1. Introduction

The water exchange reaction between the first and second coordination shell around a metal ion in aqueous solution is the simplest ligand substitution reaction (Eq. (1)). It is a fundamental reaction in understanding of the reactivity of metal ions in chemical and biological systems

$$[M(H_2O)_n]^{z+} + nH_2O^* \rightleftarrows [M(H_2O^*)_n]^{z+} + nH_2O \quad (1)$$

The replacement of a water molecule from the first coordination shell is an important step in complex formation reactions of metal cations and in many redox processes. The chemistry of aqua ions has been the subject of a recent book [1].

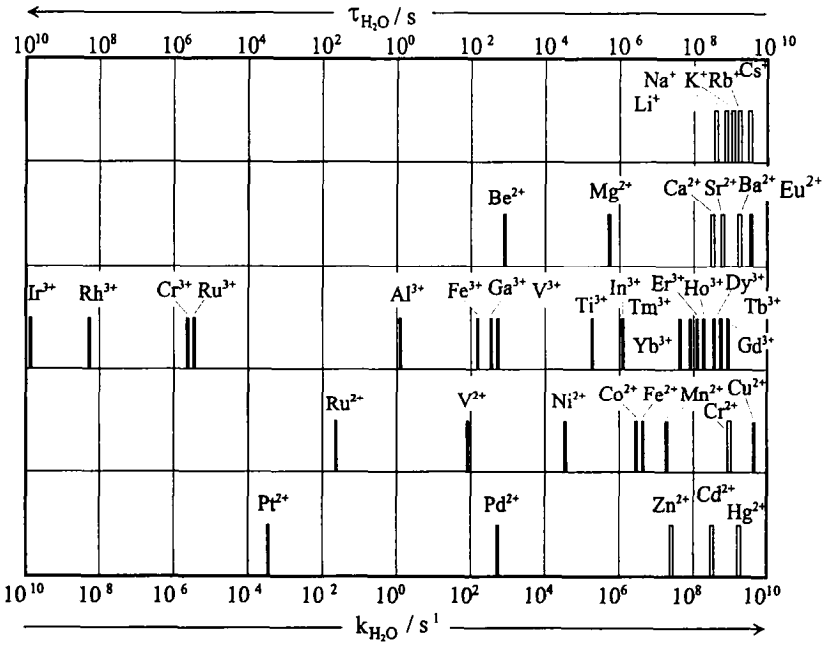

Fig. 1. Mean lifetimes of a single water molecule in the first coordination sphere of a given metal ion. τ_{H_2O}, and the corresponding water exchange rate constants, k_{H_2O}. The tall bars indicate directly determined values, and the short bars indicate values deduced from ligand substitution studies.

In water exchange reactions the reactant and the product are identical, as are the ligand and the solvent: water. The Gibbs energy change of the reaction is zero. The observed exchange rate constants cover more than 18 orders of magnitude (Fig. 1) from the most labile monovalent alkaline ions to the very inert trivalent transition metal ions Rh^{3+} and Ir^{3+} [2]. On the fast exchange side, the mean lifetime of a water molecule in the first coordination shell of Cs^+ was estimated to 200 ps. Cs^+ is the largest monovalent metal cation, and therefore, has the lowest surface charge density. On the other extreme, a water molecule stays for more than 300 years in the first shell of the hexaaqua iridium(III), a third-row transition metal with a large ligand field contribution to the activation energy.

The metal ions are often classified into three groups. The first group is represented by the main group metal ions, varying mainly in ionic radius and electric charge. The number of water molecules in the first coordination sphere spans from four to ten or more [3]. The second group consists of the d-transition metal ions, all hexa-coordinated with the exception of Pd^{2+} and Pt^{2+} which are square planar and Sc^{3+} that might be hepta-coordinated [4]. Their exchange rate constants are very strongly linked to the occupancy of their d-orbitals. The third group involves the lanthanide and actinide ions which are eight or nine coordinated. Their kinetic behavior is influenced mostly by the decrease of the ionic radius along the series and the subsequent change in the coordination number.

Experimentally, water exchange rate constants are determined mainly from nuclear magnetic resonance measurements [5,6]. Other techniques are restricted to very slow reactions (classical kinetic methods using isotopic substitution) or are indirect methods, like ultrasound absorption, where the rate constants are estimated from SO_4^{2-} complexation reactions [7]. The microscopic nature of the mechanism of the exchange reaction is not directly accessible by experimental methods. In general, reaction mechanisms can be deduced by experimentally testing the sensitivity of the reaction rate to a variety of chemical and physical parameters such as temperature, pressure, or concentration.

In recent years the application of classical molecular dynamics or Monte Carlo simulations as well as ab initio and DFT calculations have gained significant interest. The performance of the new computer generations and the theoretical approaches allows now to perform calculations which can provide deeper microscopic insight into water exchange processes. Classical simulations of hydrated metal ions in solution mainly rely on pairwise additive, effective interaction potentials obtained from quantum mechanical calculations or from empirical optimization of thermodynamic values like hydration energies or radial distribution functions. This approach limits these simulations to metal ions with filled atomic orbitals, mainly to main group ions and those transition metal ions, where ligand field effects can be neglected (e.g. lanthanides). The advantage of the classical methods is that relatively large systems, containing up to 10^3 water molecules can be simulated over several ns (10^{-9} s). Exchange processes can be followed directly by inspecting trajectories, molecular coordinates and velocities as a function of time.

Full quantum mechanical calculations using ab initio self-consistent field (SCF) methods or density functional theory are computationally much more demanding and, therefore, restricted mostly to ion–water clusters containing one metal ion and a limited number of water molecules. Different metal–water clusters that can occur along the reaction coordinate of a water exchange process have to be calculated. A comparison of energies and structural parameters like metal–oxygen bond distances in the reactants, transition states and intermediates will help to associate them to different reaction mechanisms. In gas-phase calculations, second coordination sphere, bulk solvent and anions are neglected and, furthermore, contrary to classical molecular dynamics simulations no real time-scale is provided. On the other hand, these calculations are not based on empirical pairwise interaction potentials, calculations on all types of ions, including transition metals, are feasible.

A promising method, developed in recent years, is the first principles molecular dynamics like the Car–Parrinello technique [8]. In these calculations the interatomic potentials are derived explicitly from electronic ground-state within the density functional theory in local or non-local approximation. It combines quantum mechanical calculations with molecular dynamics simulations and, therefore, overcomes the limitations of both methods. Actual computers allow only simulations of aqueous solutions of about 50 water molecules for several ps (10^{-12} s). This limit is still at least one order of magnitude shorter than the fastest directly measured water exchange rate, $k = 3.5 \times 10^9$ s^{-1} for $[Eu(H_2O)_8]^{2+}$, i.e. one exchange event every $(8 \times 3.5 \times 10^9\ s^{-1})^{-1} = 36$ ps [9].

2. Theoretical concepts of solvent exchange reactions

The mechanistic classification accepted for ligand substitution reactions was proposed by Langford and Gray in 1965 [10]. They divided substitution reactions into three categories of stoichiometric mechanisms: associative (A), where an intermediate of increased coordination number can be detected, dissociative (D) where an intermediate of reduced coordination number can be detected, and interchange (I) where there is no kinetically detectable intermediate. Furthermore, they distinguished two major categories of intimate mechanisms: those with an associative activation mode (a), where the reaction rate is approximately as sensitive to variation of the entering group as to variation of the leaving group, and those with a dissociative mode (d), where the reaction rate is much more sensitive to the variation of the leaving group than to the variation of the entering group. Evidently all D mechanisms must be dissociatively and all A mechanisms must be associatively activated. The I mechanisms include a continuous spectrum of transition states where the degree of bond-making between the incoming ligand and the complex ranges from very substantial (I_a mechanism) to negligible (I_d mechanism) [11,12]. For a solvent exchange process, the forward and backward reaction coordinates must be symmetrical. Thus, for an I_d mechanism, with negligible bond-making of the entering group, the leaving group is also necessarily weakly bound. Inversely, for an I_a mechanism, both the entering and the leaving group

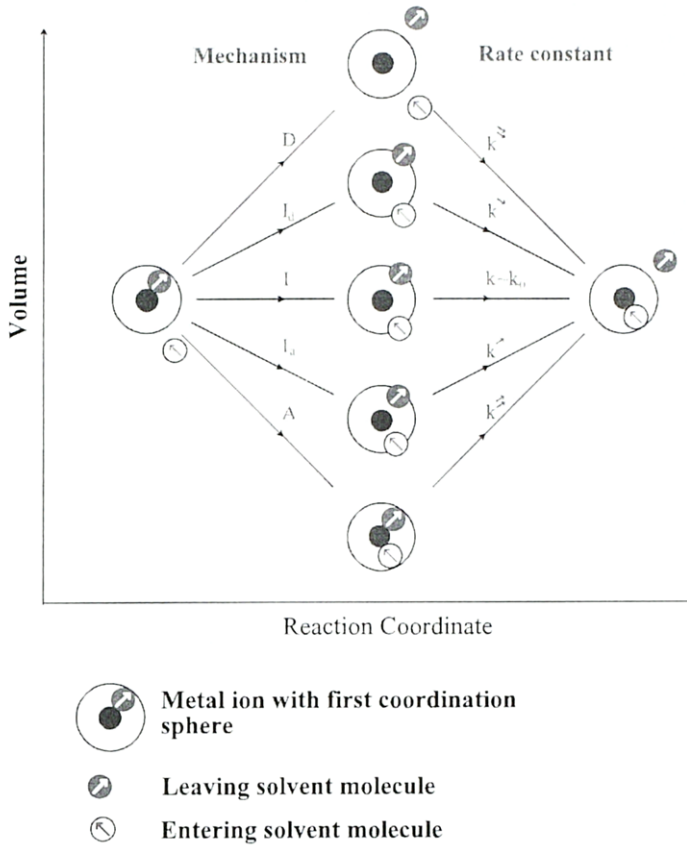

Fig. 2. Representation of the transition state for the spectrum of solvent or symmetrical ligand exchange processes.

must have a considerable bonding to the metal (Fig. 2) [11]. Swaddle suggests that for substitution of solvents such as water on octahedral complexes, only *I* mechanisms need be considered [13]. He assumes that associative *A* processes are sterically inhibited, whereas dissociative *D* mechanisms are unlikely due to the long life-times required for intermediates with a reduced coordination number (nanosecond time-scale). Furthermore, he concluded from early computer simulations [14] that there can be no clear-cut mechanistic classification of the I_a/I_d type [13] and proposed that there is just one interchange mechanism which spans an essentially infinite number of microscopic pathways. For a particular reaction a broad manifold of microscopic pathways will be more important than others, leading to a distinctive set of measurable parameters.

As above mentioned, the proposition of a reaction mechanism is based mainly on the response of the reaction rate to the variation of chemical and physical parameters. The volume of activation, $\Delta V^{\ddagger}$, has become the main tool for the

experimental identification of the water exchange mechanism [15–17]. $\Delta V^{\ddagger}$ is defined as the difference between the partial molar volume of the reactants and that of the transition state at a temperature T, and given in Eq. (2).

$$\left(\frac{\partial \ln(k)}{\partial P}\right)_T = -\frac{\Delta V^{\ddagger}}{RT} \tag{2}$$

The observed exchange rate, k, is either slowed or accelerated by increasing pressure, depending on the positive or negative sign of $\Delta V^{\ddagger}$, respectively. It is usually accepted that the activation volume has two contributions: an intrinsic component, $\Delta V^{\ddagger}_{\text{int}}$, resulting from changes in bond lengths and bond angles, and an electrostrictive component, $\Delta V^{\ddagger}_{\text{elec}}$, which arises from changes in electrostriction of the solvent outside the first coordination sphere. For solvent exchange reactions differences in electrostriction between the transition state and the reactant can be neglected, hence $\Delta V^{\ddagger} \approx \mathrm{D}V^{\ddagger}_{\text{int}}$. Consequently, the activation volume will be a direct measure of the degree of bond formation or bond breaking in the transition state. The relation between the pressure induced changes of the observed exchange rates and the underlying solvent exchange reaction mechanisms is visualized in Fig. 2. An important issue is the prediction of activation volumes for the limiting substitution mechanisms D and A. Swaddle [18,19] developed a semi-empirical model in which the absolute partial molar volume, $\Delta V^{0}_{\text{abs}}$, of a hydrated metal ion in water is related to its ionic radius, depending on the coordination number, and the charge of the metal ion. Taking ionic radii from Shannon, this model gives similar absolute limiting values of $|\Delta V^{\ddagger}| = 13.5$ cm^3 mol^{-1} for D and A processes on di- and trivalent 3d transition metal ions.

3. Water exchange from the first coordination shell

3.1. Transition metal ions

Water exchange on di- and trivalent transition metal ions has been the subject of extensive experimental studies and has been widely reviewed [11,20]. Table 1 summarizes the experimental first-order rate constants and the activation parameters. The sequence of reactivity of the divalent first-row transition metal ions is largely independent of the mechanism and semi-quantitatively coincides with predictions based on ligand field activation energies and molecular orbital calculations [20–22].

The water exchange mechanism progressively changes from I_a to I_d as the number of d-electrons increases and the ionic radius decreases. This change is demonstrated most evidently by the change in sign of the activation volume, $\Delta V^{\ddagger}$. The observed progressive mechanistic changeover cannot be explained in terms of cationic size only, the electronic configuration also plays an important role. For a σ-bonded octahedral complex, the t_{2g} orbitals are non-bonding, whereas the e_g orbitals are antibonding. The gradual filling of the t_{2g} orbitals, spread out between ligands, will electrostatically disfavor the approach of a seventh molecule towards

Table 1
Rate constants and activation parameters for water exchange on transition metal ions

Ion	Geometry	k (298K) (s^{-1})	$\Delta H^{\ddagger}$ (kJ mol^{-1})	$\Delta S^{\ddagger}$ (J K^{-1} mol^{-1})	$\Delta V^{\ddagger}$ (cm^3 mol^{-1})	Mechanism	Ref.
$[V(H_2O)_6]^{2+}$	Octahedral	8.7×10^{1}	61.8	−0.4	−4.1	I_a	[23]
$[Mn(H_2O)_6]^{2+}$	Octahedral	2.1×10^{7}	32.9	+5.7	−5.4	I_a	[24]
$[Fe(H_2O)_6]^{2+}$	Octahedral	4.4×10^{6}	41.4	+21.2	+3.8	I_d	[24]
$[Co(H_2O)_6]^{2+}$	Octahedral	3.2×10^{6}	46.9	+37.2	+6.1	I_d	[24]
$[Ni(H_2O)_6]^{2+}$	Octahedral	3.2×10^{4}	56.9	+32.0	+7.2	I_d	[24]
$[Cu(H_2O)_6]^{2+}$	Dist. Octahed.	4.4×10^{9}	11.5	−21.8	+2.0	I_d	[22]
$[Ru(H_2O)_6]^{2+}$	Octahedral	1.8×10^{-2}	87.8	+16.1	−0.4	I_d	[31]
$[Pd(H_2O)_6]^{2+}$	Square planar	5.6×10^{2}	49.5	−26	−2.2	I_a	[35]
$[Pt(H_2O)_4]^{2+}$	Square planar	3.9×10^{-4}	89.7	−9	−4.6	I_a	[36]
$[Ti(H_2O)_6]^{3+}$	Octahedral	1.8×10^{5}	43.4	+1.2	−12.1	A, I_a	[25]
$[V(H_2O)_6]^{3+}$	Octahedral	5.0×10^{2}	49.	−27.8	−8.9	I_a	[26]
$[Cr(H_2O)_6]^{3+}$	Octahedral	2.4×10^{-6}	108.6	+11.5	−9.6	I_a	[27]
$[Fe(H_2O)_6]^{3+}$	Octahedral	1.6×10^{2}	64.0	+12.1	−5.4	I_a	[28,29]
$[Ga(H_2O)_6]^{3+}$	Octahedral	4.0×10^{2}	67.1	+30.1	+5.0	I_d	[30]
$[Ru(H_2O)_6]^{3+}$	Octahedral	3.5×10^{-6}	89.8	−48.3	−8.3	I_a	[31]
$[Rh(H_2O)_6]^{3+}$	Octahedral	2.2×10^{-9}	131.2	+29	−4.2	I_a	[33]
$[Ir(H_2O)_6]^{3+}$	Octahedral	1.1×10^{-10}	130.5	+2.1	−5.7	I_a	[2]

a face of the octahedron, and therefore decrease the ease of bond-making. Similarly, an increased occupancy of the e_g orbitals, pointed to the ligands, will enhance the bond breaking tendency. These effects, combined with the steric effects outlined above, can explain the sequences of the $\Delta V^{\ddagger}$ values.

The very high lability of the d^9 $[Cu(H_2O)_6]^{2+}$ is coincident with the operation of a dynamic Jahn–Teller effect [23]. Its tetragonal distortion reorients randomly very rapidly so that the lifetime of a given distortion ($\tau_i = 5.1 \times 10^{-12}$ s at 298 K) is much shorter than the lifetime of a given coordinated H_2O molecule ($t_{H_2O} = 2.3 \times 10^{-10}$ s at 298 K). The longer axial bonds facilitate water exchange through a d-activation mode which is consistent with the positive activation volume (Table 1).

Water exchange on trivalent first-row transition metal ions shows a similar behavior as that of the divalent analogues. $[Cr(H_2O)_6]^{3+}$ is the most inert (Table 1) as a consequence of its large ligand field activation energy reflected in the large $\Delta H^{\ddagger}$ value. $\Delta V^{\ddagger}$ decreases from -12.1 ($[Ti(H_2O)_6]^{3+}$) to -5.4 cm^3 mol^{-1} ($[Fe(H_2O)_6]^{3+}$). The activation volume for Ti^{3+} approaches the limiting value of -13.5 cm^3 mol^{-1} for an A mechanism [18], hence the operation of an A mechanisms can be assigned. As the occupancy of the t_{2g} orbitals and in parallel the electronic repulsion towards an entering ligand increase, the activation volumes become less negative, indicating a changeover to less associative, and finally a dissociative activation mode (for Ga^{3+}) as a consequence of the filling of the σ anti-bonding e_g orbitals.

Experimental data on water exchange on second- and third row transition metal ions are much more scarce. The mechanism of water exchange on octahedral $[Ru(H_2O)_6]^{2+}$ has been discussed from different aspects. Based on the small activation volume, $\Delta V^{\ddagger} = -0.4$ cm^3 mol^{-1}, an interchange, I, mechanism was first attributed [32]. The mechanism of the substitution reactions on $[Ru(H_2O)_6]^{2+}$ has been determined by comparing the rate constants for the monocomplex formation between the aqua ion with different ligands [33]. The extreme similarities between the inner sphere interchange rate constants, k_i, for a series of complex formation reactions let the authors assign a dissociative interchange mechanism, I_d. The small activation volume may originate from the compensation between a positive contribution due to the loss of a water molecule and a negative term from the contraction of the complex at the transition state. The low-spin t_{2g}^5 $[Ru(H_2O)_6]^{3+}$ is four orders of magnitude more labile than the t_{2g}^6 $[Ru(H_2O)_6]^{2+}$ [32]. This difference in lability led to the unequivocal identification of an outer-sphere mechanism operating in the electron exchange between these two aqua complexes [32]. $[Rh(H_2O)_6]^{3+}$ and its third-row analog $[Ir(H_2O)_6]^{3+}$ are the most inert aqua ions known up to now [2,34]. The lifetime of a water molecule in the first coordination shell of Ir^{3+} is 9.1×10^9 s (at 298 K), which corresponds to about 300 years. The negative activation volumes of the Ru^{3+}, Rh^{3+} and Ir^{3+} ions suggest the operation of an associative I_a exchange mechanism.

The vast majority of the square-planar d^8 transition metal ions, such as palladium(II) and platinum(II) undergo ligand substitution through associatively activated mechanisms [35]. Water exchange on $[Pd(H_2O)_4]^{2+}$ [36] and $[Pt(H_2O)_4]^{2+}$ [37] were studied by ^{17}O NMR (Table 1). The mechanistic interpretation of the activation

volumes is complicated by the square-planar geometry of the complexes. The axial sites may be occupied by non-bonded water molecules. The bond formation between the metal center and such a water molecule leading to a five-coordinate transition state may result in rather small volume changes. It is therefore difficult to distinguish from $\Delta V^{\ddagger}$ values between an associative interchange I_a and a limiting associative A mechanism.

In recent years, several authors published ab initio or density functional theory (DFT) calculations on gas-phase hydrated metal ions. The main goal of the studies was to obtain microscopic insight into water exchange on octahedral complexes. On constrained pentagonal bipyramidal heptacoordinated species of the type $[M(H_2O)_7]^{n+}$, Åkesson et al. [38] obtained an interchange water exchange mechanism with increasingly associative character in the order Cr^{3+}, Fe^{3+}, V^{3+} and Ti^{3+}, which is consistent with experimental activation volumes. However, they proposed a dissociative mechanism for water exchange on octahedral Mn^{2+} and V^{2+} ions, which is in contradiction with experimental findings. This discrepancy was resolved by Rotzinger [39–41] who performed calculations on di- and trivalent first-row transition metal ions from Sc^{3+} to Zn^{2+} using ab initio methods at the Hartree–Fock or CAS–SCF level. All pertinent transition states and intermediates that could occur along the reaction coordinate of an associative, a concerted and a dissociative water exchange process were calculated. In this study, reactants, products, and intermediates were characterized by the absence of any imaginary vibrational frequency throughout, whereas transition states always show a single imaginary frequency [39]. As an approximation, he neglected second sphere and bulk water as well as anions. The reliability of his calculations was proved by the agreement of the computed activation energies $\Delta E^{\ddagger}$ with the experimental $\Delta G^{\ddagger}$ and $\Delta H^{\ddagger}$ values.

The computations provided structures and energies for a variety of transition states and intermediates for water exchange. Each type of exchange mechanism proceeds via a characteristic transition state. As examples we will discuss Rotzinger's results for Ti^{3+}-, V^{2+}- and Ni^{2+}- clusters. The calculated transition state of Ti^{3+} (Fig. 3a) has C_1 symmetry. The imaginary frequency describes a

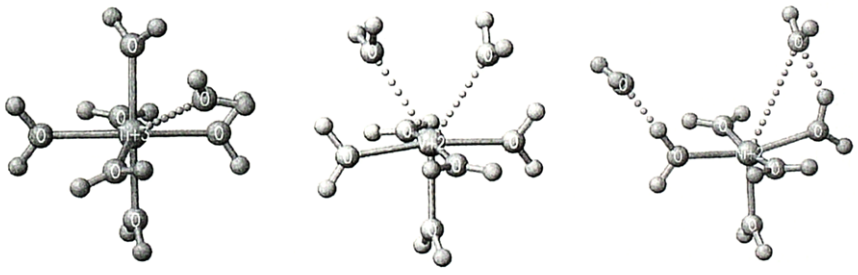

(a) (b) (c)

Fig. 3. Perspective views of the $\{[Ti(H_2O)_6\cdots(H_2O)]^{3+}\}^{\ddagger}$ transition state (a), $\{[V(H_2O)_5\cdots(H_2O)_2]^{2+}\}^{\ddagger}$ transition state (b) and $\{[Ni(H_2O)_5\cdots H_2O{\cdot}H_2O]^{2+}\}^{\ddagger}$ transition state (c).

motion of the seventh water molecule toward or away from the metal center. As Rotzinger states, in this reaction water entry dominates undoubtedly the activation process which can clearly be identified as an *A* mechanism. The following heptacoordinated intermediate $[Ti(H_2O)_7]^{3+}$ has only real vibrational modes and C_1 symmetry. The calculated energies of the transition state and the intermediate are given in Fig. 4, together with the experimental $\Delta G^{\ddagger}$ value. Calculation of the partial molar volumes of the reactants, the transition state and the intermediate is difficult and Rotzinger calculated differences of the sums of all metal–oxygen bond lengths, $\Delta\Sigma$, which are related to the activation volumes. Fig. 4 shows that the sign of $\Delta\Sigma$ is negative and agrees with that of the experimental $\Delta V^{\ddagger}$.

The transition state for $\{[V(H_2O)_5\cdots(H_2O)_2]^{2+}\}^{\ddagger}$ (Fig. 3b) has C_2 symmetry and is arising from a concerted process. The entering and the leaving ligands are symmetrically equivalent and indistinguishable. The hypothetical transition states involving electronic low-spin (triplet) states, $\{[V(H_2O)_7]^{2+}\}^{\ddagger}$, have very high energies (242 and 244 kJ mol^{-1}) relative to the reactant, excluding spin-change in the water exchange process. The negative value of $\Delta\Sigma$ for the transition state shows that bond formation occurs to a larger extent than bond breaking. This is representative for an I_a mechanism which was previously attributed form high-pressure experiments.

For water exchange on $[Ni(H_2O)_6]^{2+}$ only a transition state for the dissociative activation could be calculated. The species $\{[Ni(H_2O)_5\cdots(H_2O)\cdot(H_2O)]^{2+}\}^{\ddagger}$ (Fig. 3c) has C_s symmetry and the incoming and the leaving water molecules are well distinguishable. The imaginary modes involve mainly a motion of the leaving ligand toward or away from Ni^{2+}. The subsequent intermediate $[Ni(H_2O)_5\cdot(H_2O)_2]^{2+}$ has C_{2v} symmetry and is basically a square-pyramidal penta-coordinate species, hydrated by two water molecules. The calculated sum of the metal–oxygen bonds has increased for both the transition state and the intermediate as compared to the reactant leading to a positive of value $\Delta\Sigma$ (Fig. 4). The energy difference between transition state and intermediate is small for this dissociative process. An improved model could change the energies of the intermediate and the transition state in an unequal way, so that the pentacoordinated intermediate becomes the transition state for an I_d mechanism.

In summary, the results obtained by Rotzinger on first row transition metals provided the following picture [40]. Hexacoordinated Sc^{3+}, Ti^{3+} and V^{3+} react via an associative *A* mechanism with relatively long-lived intermediates. The dissociative pathway is the only possible for water exchange on Ni^{2+}, Cu^{2+} and Zn^{2+}. For the elements in the middle of the 3d series both associative (I_a/A) and dissociative (D) pathways can occur.

The hydration of the zinc(II) ion was also studied by Hartmann et al. [42]. Structures and hydration energies were computed using DFT for $[Zn(H_2O)_n]^{2+}$ with $n = 1$–6 and for $[Zn(H_2O)n]^{2+}\cdot mH_2O$ with $n = 5$ and $m = 1$, 2 and $n = 6$ and $m = 1$. The structures with water molecules in the second coordination sphere revealed two types of complexes having either one or two hydrogen bonds between the first and second sphere water molecules. In agreement with Rotzinger [40], a dissociative *D* mechanism was found to be most likely for the water exchange on $[Zn(H_2O)_6]^{2+}$.

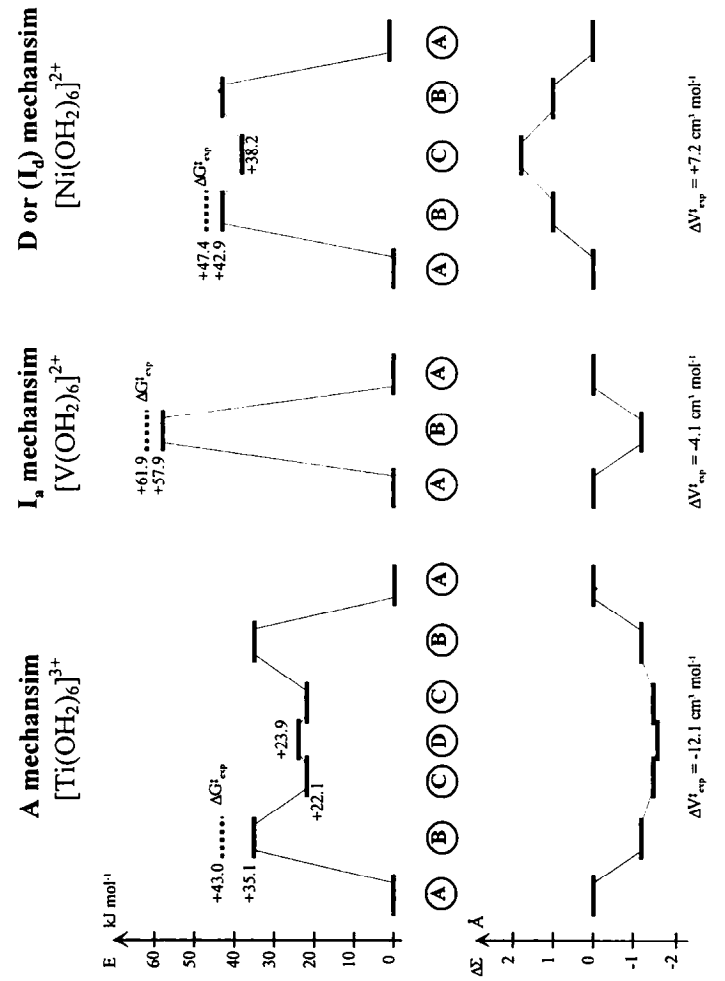

Fig. 4. Energy (top) and bond length difference/volume (bottom) profiles for an *A* mechanism (left), I_a mechanism (middle) and *D* mechanism (right).

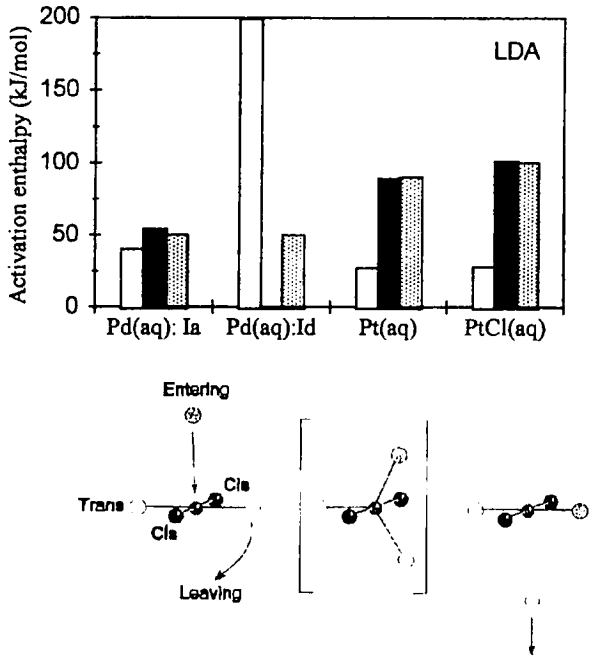

Fig. 5. Calculated and observed activation enthalpies obtained for an associative mechanism on $[Pd(H_2O)_4]^{2+}$, a dissociative mechanism on $[Pd(H_2O)_4]^{2+}$, and for associative mechanisms on $[Pt(H_2O)_4]^{2+}$, and $[Pt(H_2O)Cl_2]^{2+}$ (top). The black bars include relativistic contributions computed at the LDA geometries, the white bars refer to nonrelativistic results, and the shaded boxes represent observed values. Schematic representation of the ligand exchange process on planar d^8 aqua complexes (bottom).

Density functional theory has been used by Deeth et al. [43] to model water exchange on square-planar $[Pd(H_2O)_4]^{2+}$ and $[Pt(H_2O)_4]^{2+}$. Energies and structures of three-, four- and five-coordinated species were calculated. In order to reproduce experimental activation enthalpies, $\Delta H^{\ddagger}$, for water exchange, an explicit correction for solvation was applied by using the simple Born model. The calculations strongly suggest that water exchange at these square-planar metal centers proceeds via an associative mechanism, in full agreement with experimental assignments [36,37]. The agreement in experimental and calculated activation enthalpy is better than 10 kJ mol^{-1} for an I_a mechanism, whereas it differs for more than 100 kJ mol^{-1} for an I_d mechanism. Fig. 5 shows a schematic representation of the water exchange process on planar d^8 complexes. The transition state has a structure close to a trigonal bipyramid with three elongated bonds (equatorial water molecules) and two bonds of the same length as the square-planar complex. The calculations result in almost the same structure for $\{[Pd(H_2O)_5]^{2+}\}^{\ddagger}$ and for $\{[Pt(H_2O)_5]^{2+}\}^{\ddagger}$. The bond stretching in the transition states partially compensates the decrease of the molar volume originating from the association of a fifth water molecule to the metal center. This effect qualitatively explains the small and similar experimental activation volumes [36,37] for these square-planar aqua complexes (Table 1).

3.2. Lanthanides

The 15 trivalent lanthanide ions, which may be collectively denoted Ln^{3+}, represent the most extended series of chemically similar metal ions. The progressive filling of the 4*f* orbitals from La^{3+} to Lu^{3+} is accompanied by a smooth decrease in ionic radius with increase in atomic number as a consequence of the increasingly strong nuclear attraction for the electrons in the diffuse f orbitals. These orbitals are shielded by the surrounding filled 5s and 5p orbitals, leading to very small crystal field splittings in the lanthanide complexes. Thus, the coordination properties of the Ln^{3+} ions mainly depend upon the steric and electrostatic nature of the ligands. The coordination of the lanthanide(III) ions in aqueous solution was certainly one of the most controversial questions of lanthanide chemistry. Now it is well established from neutron scattering [44,45], X-ray scattering [46–48] and absorption fine structure [49], density [50] and spectrophotometric [51] techniques that the lighter ions (La^{3+}–Nd^{3+}) are predominantly nine-coordinate and the heavier ions (Gd^{3+}–Lu^{3+}) are predominantly eight-coordinate species. The ions Sm^{3+}–Eu^{3+} exist in equilibria between nine- and eight-coordinate. The change in coordination number is reflected in the absolute partial molar volumes, V^0_{abs}, determined in aqueous $LnCl_3$ solutions (Fig. 6).

$$[Ln(H_2O)_8]^{3+} + H_2O \rightleftarrows [Ln(H_2O)_9]^{3+} \quad (3)$$

The calculated absolute partial molar volumes using the semi-empirical model of Swaddle [18,19] agree well with $[Ln(H_2O)_9]^{3+}$ at the beginning and with $[Ln(H_2O)_8]^{3+}$ at the end of the Ln^{3+}-series.

The absence of crystal field splitting and the shielding of the f orbitals makes classical molecular dynamics simulations feasible. Hence, for solvents without covalent bonding like water, ion–solvent forces can be well represented by simple Coulomb and van der Waals terms. Due to the strong electric field of the trivalent ions, water molecules in the first coordination shell are polarized. Inclusion of a polarization term proved to be essential in the description of the Ln^{3+}-water interaction (Fig. 7) [52].

Fig. 8 shows the distribution of the number of water molecules for three distance regions of three trivalent ions, designed as Nd^{3+}, Sm^{3+} and Yb^{3+} [52]. The first and the second hydration shells as well as the region between the two shells were obtained from classical molecular dynamics simulations using one cation immersed in 300 polarizable water molecules. The experimentally observed change of the first shell coordination number CN_1 from nine for Nd^{3+} to eight for Yb^{3+} could be reproduced. The result for Sm^{3+} reveals that the observed CN_1 of 8.5 corresponds indeed to an equilibrium between an octa aqua and an ennea aqua ion. Only 9% of all configurations have a ninth water molecule between the two spheres (Fig. 8).

An advantage of computer simulations is that they can deliver microscopic structural pictures of the systems studied. A detailed analysis of the first coordination shell [53] showed that for the light lanthanide ions (Nd^{3+}) the nine water molecules form a tricapped trigonal prism (Fig. 9) similar to that found by solid state X-ray diffraction studies on $[Ln(H_2O)_9]^{3+}$ with counterions $CF_3SO_3^-$,

$EtOSO_3^-$, and BrO_3^- [54]. The mean ion–oxygen distance, r_M, calculated for the three capping water molecules is 3.6% longer than that for the six prismatic ones. The eight H_2O molecules in contact with the smaller heavy lanthanide ions (Yb^{3+}) form a square antiprismatic geometry (Fig. 9) with equal ion–oxygen distances. The dipole vectors of the first coordination shell water molecules are radially aligned [52] with mean tilt angles from the cation–oxygen axis of 13° (Nd^{3+}, Sm^{3+}) and 12° (Yb^{3+}). The distribution function of all angles $\theta = \angle O'\text{–ion–}O''$, formed by pairs of water oxygens that belong to the first shell, was calculated and agreed well with the structures described above [53].

As already mentioned, hydration shells from simulations of Sm^{3+} are actually a mixture of equal amounts of eight- and nine-fold coordinated ions. If water

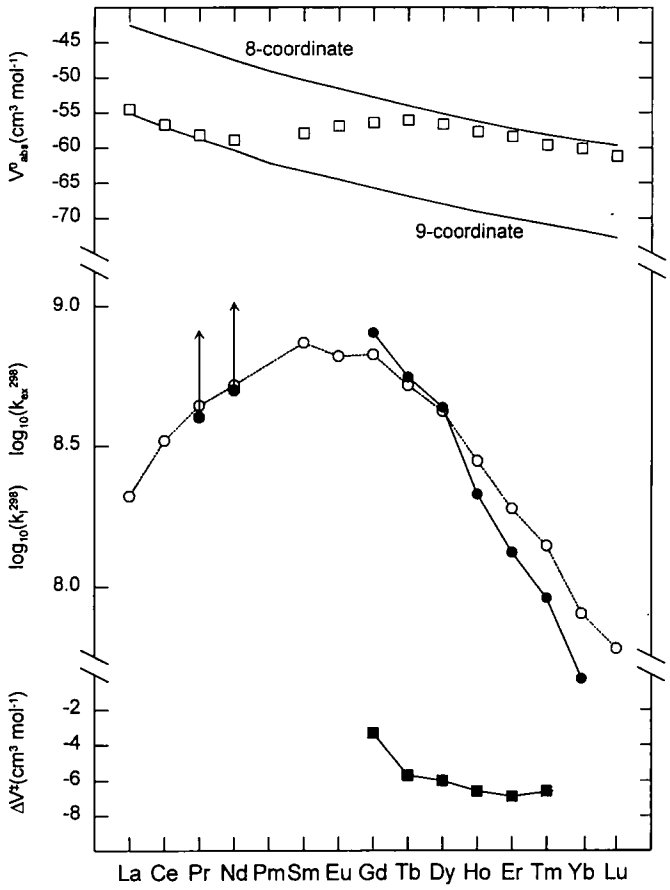

Fig. 6. Absolute partial molar volumes, V^0_{abs}, of $[Ln(H_2O)_n]^{3+}$ in aqueous $LnCl_3$ solutions (□), compared with the calculated values for $[Ln(H_2O)_8]^{3+}$ and $[Ln(H_2O)_9]^{3+}$ indicated by the upper and lower solid curves respectively. Interchange rate constants, k_i, for the substitution of SO_4^{2-} on $[Ln(H_2O)_n]^{3+}$ are shown as ○, and water exchange rate constants, (298 K) for $[Ln(H_2O)_8]^{3+}$ are shown as ●. Activation volumes, $\Delta V^{\ddagger}$, are shown as ■.

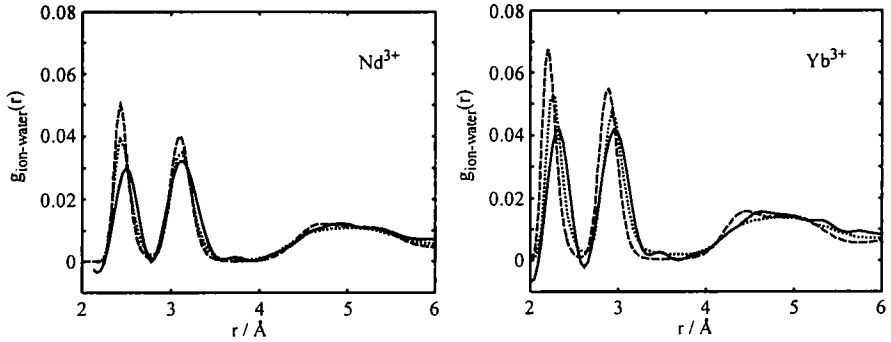

Fig. 7. Comparison of the Ln^{3+}–water oxygen radial distribution function, g_{M-O}, from the simulations (··· unpolarizable water,---polarizable water) with experimental data from neutron diffraction for Nd^{3+} and Yb^{3+} (— experimental data).

molecules up to an ion–oxygen distance of 3.0 Å are considered, either a tricapped trigonal prism (for $CN_I = 9$) or a square antisprim (for $CN_I = 8$) is found. Fig. 10 (bottom) gives an example of the trajectories of the water molecules of the first and the second hydration shell for a 100 ps interval and illustrates the equilibrium between the two coordinations. The reaction volume, ΔV^0, for this equilibrium can be estimated from geometrical considerations. Using Swaddle's semi-empirical model [18] a volume of -13.0 cm^3 mol^{-1} can be calculated. From the molecular dynamics simulations volumes included in the solvent-accessible Connolly surface [55], V_{sas}, can be calculated. In Fig. 10 (top) the Connolly volume enclosed by the surface of the first hydration shell of the Sm^{3+} aqua ion is given as a function of time. With V_{sas} ($CN_I = 9$) = 112.0 cm^3 mol^{-1} and V_{sas} ($CN_I = 8$) = 101.2 cm^3 mol^{-1} a reaction volume of -7.2 cm^3 mol^{-1} was calculated [56]. Molecular dynamics simulations performed at different densities ($\rho = 0.9$, 1.0 and 1.1 g cm^{-3} corresponding to pressures of -2440, 1 and 1880 bar) showed a change in the mean coordination number from 8.26 to 8.62 due to an increase of configurations with nine coordinated water molecules in the first shell with increasing density (Fig. 11). The slope of a plot of ln(K) versus the pressure gives DV^0 [56]. The value obtained in this way (-8.3 cm^3 mol^{-1}) is close to the one described above; both volumes calculated in different manners from MD simulations agree well with the reaction volume of -10.9 cm^3 mol^{-1} measured experimentally for $[Ce(H_2O)_8]^{3+} + H_2O \rightleftarrows [Ce(H_2O)_9]^{3+}$ [57].

Rate constants for water exchange on lanthanide(III) ions can be determined by ^{17}O-NMR relaxation and chemical shift measurements [58,59]. Unfortunately, only eight-coordinate heavy lanthanides (Gd^{3+} to Yb^{3+}) could be studied (Fig. 6). Powell's results [60] at high magnetic fields allow to determine lower limits for water exchange rates at 298 K on $[Nd(H_2O)_9]^{3+}$ and $[Pr(H_2O)_9]^{3+}$. The water exchange rates are closely correlated with the rate, k_i^{298}, of the interchange between an inner sphere water molecule and a SO_4^{2-} ion from the outer sphere coordination (Fig. 6) [61]. The values show a maximum in the middle of the series, corresponding

to the crossover region in CN_I from nine to eight. For the heavy lanthanides, in addition to variable temperature, variable pressure measurements were made so that the activation volumes for the exchange process could be determined. The activation volumes are all negative [59], indicating an associatively activated water exchange mechanism (Fig. 6). This observation can be explained in terms of the coordination equilibrium observed in the middle of the series. For the heavy lanthanides, the octa ion is the lowest energy species and the ennea aqua ion represents the intermediate (or transition state) in the associatively activated water exchange reaction. The exchange rates become faster towards the middle of the series as the difference in the energy between octa aqua and ennea aqua ions decreases. For the mid-series lanthanides, the octa and the ennea- aqua species are in equilibrium. The transition from one species to the other requires relatively little energy, so that these lanthanides should have the fastest water exchange rates of the series. For the light lanthanides, the ennea aqua ion is now the lowest energy

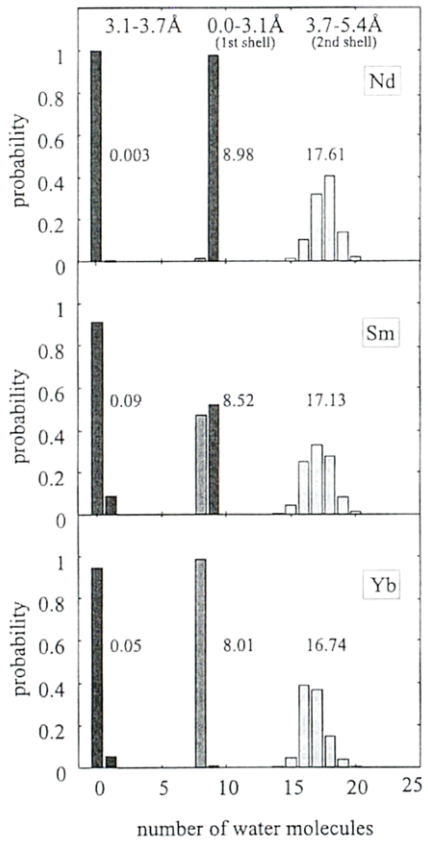

Fig. 8. Distribution of the number of H_2O molecules in three distance regions for the simulations, Nd, Sm, and Yb within the polarizable water model. The inserted numbers are the mean number of water molecules in each distance range.

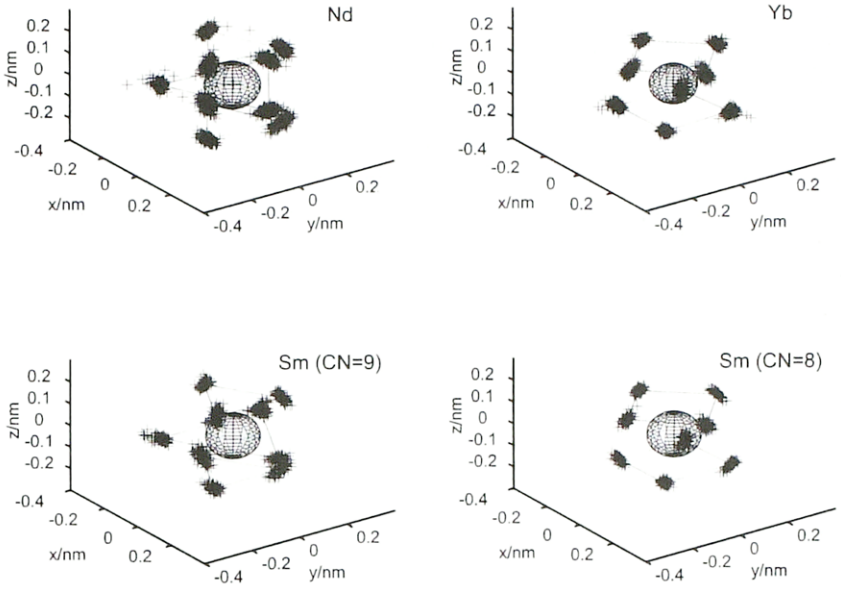

Fig. 9. Structures of the first hydration shells for the simulations Nd, Sm, and Yb. The geometric centers of the point clouds have been connected to guide the eye. The radii of the central spheres represent the ionic radii.

species. One can expect, therefore, that the octa aqua ion will be the intermediate (or transition state) in the exchange process, which will proceed via a dissociatively activated mechanism. One would expect to observe an increase in water exchange rates and positive activation volumes from La^{3+} to Nd^{3+}. Unfortunately, so far it has not proved possible to demonstrate experimentally these predictions for the light lanthanide ions.

From molecular dynamics simulations, however, information on water exchange is available for the three regions of coordination. The simulation qualitatively confirmed the lability maximum of the first hydration shell found in the middle of the series [56]. From the trajectories obtained from the simulations, all transitions of water molecules between the first hydration shell and the bulk were identified and grouped into pairs of water molecules that together form a coupled exchange (Fig. 12) [56].

The 15 exchange events on $[Nd(H_2O)_9]^{3+}$ observed in the 3.1 ns simulation time are of dissociative character throughout the simulation (Fig. 12, left). A considerable mechanistic variability between the two limiting reaction pathways is evident. One limit is a pathway with rather strong dissociative character via an eight-fold-coordinated transition state of a lifetime of 10 ps. The other extreme is a pathway with nearly synchronous leaving and entering of water molecules. Since the crossing point between the trajectory of the incoming and the leaving water molecules is displaced towards the second shell, this pathway is most appropriately classified as a dissociative interchange, I_d, mechanism with weak dissociative character. The

leaving water molecule is in any case sitting in the capping position. The remaining eight water molecules adopt a square antiprismatic geometry. The incoming water molecule approaches with the least steric hindrance by the opposite square face. The angular distribution for the angle formed by the incoming water molecule, the ion and the leaving water molecule shows a maximum at about 180°.

The water exchange on $[Yb(H_2O)_8]^{3+}$ starts with the approach of a ninth water molecule on one of the squares of the square antiprismatic geometry. After a slight rearrangement of the eight other H_2O molecules, the nine form together a tricapped trigonal prism with the incoming one sitting on a capping position. Subsequently another capping water molecule is driven out of the primary hydration shell. The oxygen-ion-oxygen angle between the incoming water oxygen, the Yb^{3+} and the leaving water oxygen is about 120° [56].

Similarly to the hydration equilibrium of Sm^{3+}, volume profiles for water exchange processes can be obtained using Connolly's method. Volume changes with respect to the mean volume of an aqua ion in equilibrium plus one isolated water molecule are shown for 10 ps intervals in Fig. 13 [56]. For $[Nd(H_2O)_9]^{3+}$ (Fig. 13, top) the dissociation of a water molecule from the primary hydration shell corresponds to an increase in volume. The picture that emerges from the volume

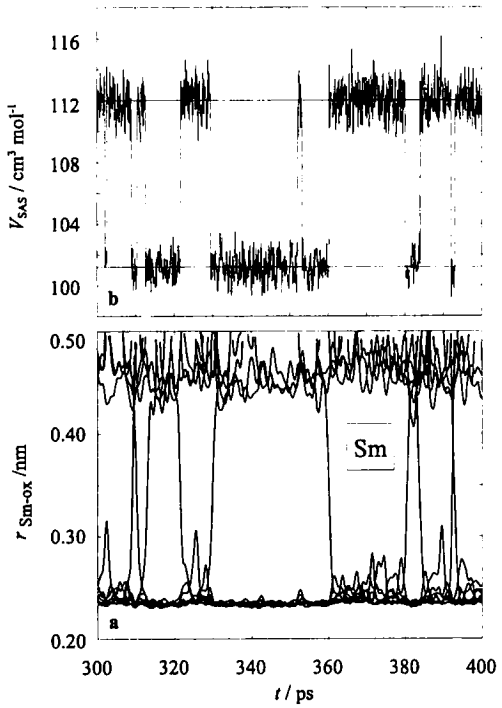

Fig. 10. Ion–oxygen distance for a 100 ps interval simulation for Sm (bottom). The plot illustrates the equilibrium between eight- and ninefold coordination. The volume V_{sas} that is enclosed by the solvent-accessible surface of the $[Sm(H_2O)_{8,9}]^{3+}$ aqua ion is shown as a function of time (top).

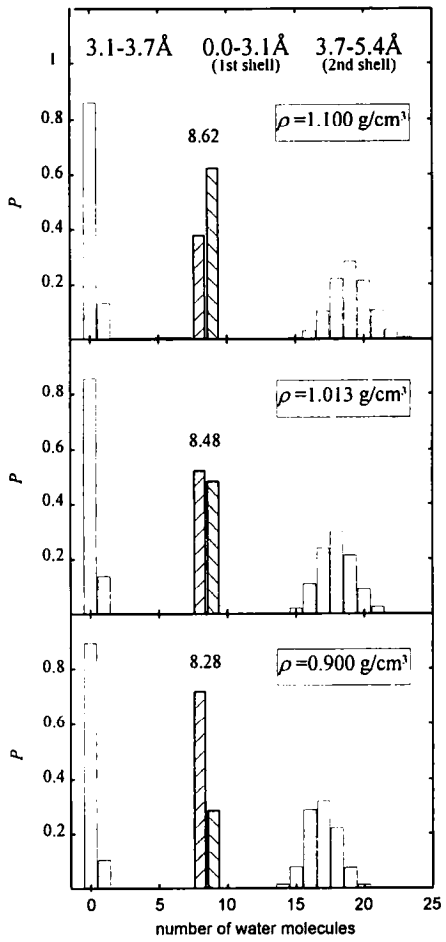

Fig. 11. Distribution of the water molecules in three distance ranges around the Sm^{3+} ion at three different overall densities. The inserted numbers are the mean numbers of water molecules in each distance range.

profile for the water exchange on $[Yb(H_2O)_8]^{3+}$ is more complicated. The entering of a water molecule from the second hydration shell into the region between the first and second sphere leads to a slight increase of the volume. This feature of the volume profile indicates that the square antiprismatic octa aqua ion prepares itself geometrically for the reception of a ninth water molecule before compacting to the transition state that is a tricapped trigonal prism.

3.3. Main group elements

There are only few main group metal ions amenable to detailed mechanistic study of water exchange: Be^{2+}, Mg^{2+}, Al^{3+}, Ga^{3+} and In^{3+}. They provide the

opportunity to study the influence of size and charge on mechanism without the complicating effects of the variation of the electronic occupancy in the d-orbitals.

All alkali ions and Ca^{2+}, Sr^{2+} and Ba^{2+} are very labile as a consequence of their relatively low surface charge density. The only direct experimental data on water exchange on some of these ions come from incoherent quasi-elastic neutron scattering (IQUENS) [62–64]. IQENS has an observation time scale $t_{obs} \sim 10^{-9}$ s and allows to give limits for ion to water-proton binding times τ_i (Table 2).

The tetrahedrally [65–69] coordinated beryllium(II) and the octahedrally [70–75] coordinated magnesium(II) show relatively slow water exchange rates from the first coordination sphere and can be measured directly by NMR techniques (Table 3). The water exchange reaction on beryllium(II) is characterized by the most negative activation volume observed for a water exchange process ($\Delta V^{\ddagger} = -13.6$ cm^3 mol^{-1}), which is close to a calculated limiting $\Delta V^{\ddagger} = -12.9$ cm^3 mol^{-1} for an A mechanism (hexa-aqua ion) [65]. The water exchange rate for $[Mg(H_2O)_6]^{2+}$ [76] lies between those of $[Co(H_2O)_6]^{2+}$ and $[Ni(H_2O)_6]^{2+}$ (Table 1) and reflects the order of ionic radii of these three ions ($Co^{2+} = 74$ pm, $Mg^{2+} = 72$ pm, $Ni^{2+} = 69$ pm) [77]. The strongly positive activation volume ($\Delta V^{\ddagger} = +6.7$ cm^3 mol^{-1}) is intermediate between those obtained for Co^{2+} and Ni^{2+}. Based on the similarity between Mg^{2+} and these ions an I_d or D mechanism is proposed for H_2O exchange. Furthermore, the complex formation rates [78] are close to the water exchange rate, which is indicative of a metal–water bond rupture as the rate determining step.

The trivalent cations Al^{3+}, Ga^{3+} and In^{3+} have closed shell configurations and differ strongly in their ionic radii (53, 62 and 80 pm, respectively). They form octahedral $[M(H_2O)_6]^{3+}$ subunits in the solid alums $CsM^{III}[SO_4]_2 \cdot 12H_2O$ [79]. In aqueous solution the coordination numbers are also six as revealed by X-ray diffraction for Al(III) [80–82] and In(III) [83–85], and by NMR measurements for Al(III) [85–87], Ga(III) [85–90] and In(III) [85]. Rate constants and activation parameters for water exchange on Al(III) [91] and Ga(III) [92,31] have been determined from kinetic ^{17}O-NMR experiments (Table 4). Water exchange processes on $[Al(H_2O)_6]^{3+}$ and $[Ga(H_2O)_6]^{3+}$ are characterized by positive $\Delta V^{\ddagger}$ values,

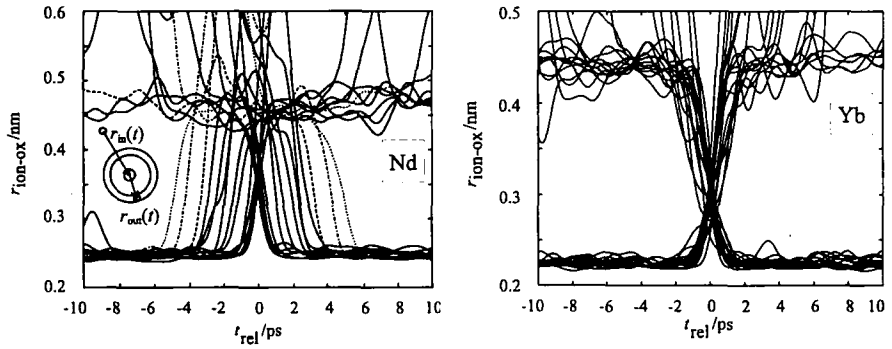

Fig. 12. Superpositions of the trajectories for the exchange events observed for solution Nd (CN = 9, left,) and for the exchange events observed for simulation Yb (CN = 8, right).

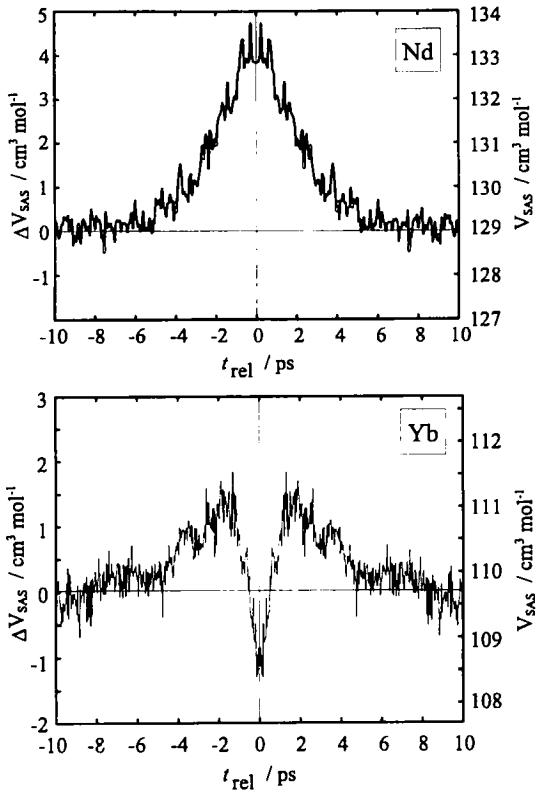

Fig. 13. Mean activation volume profile $\Delta V_{sas}(t)$ from the water exchanges on Nd^{3+} (CN = 9, (top) and Yb^{3+} (CN = 8, (bottom) after averaging the positive and the negative halves of the profile.

which are, however, substantially smaller than anticipated for a *D* mechanism, and, therefore, an I_d mechanism was proposed. Unfortunately, the water exchange rate on In^{3+} was too fast to be measured, and thus precluded the measurement of an

Table 2
Ion–water proton binding times, τ_i, obtained from IQENS experiments on concentrated aqueous ionic solutions at ~298 K [63]

$\tau_i < 10^{-10}$ s	$\tau_i > 10^{-10}$ s	$\tau_i > 5 \times 10^{-9}$ s
Li^+	Zn^{2+}	Mg^{2+}
Cs^+	Nd^{3+}	Ni^{2+}
Ca^{2+}	Dy^{3+}	Al^{3+}
Cu^{2+}		Cr^{3+}
F^-		Fe^{3+}
Cl^-		Ga^{3+}
I^-		
ClO_4^-		

Table 3
Water exchange rate constants and activation parameters for water exchange on $[Be(H_2O)_4]^{2+}$ $[Mg(H_2O)_6]^{2+}$

Ion	k (298 K) (s^{-1})	$\Delta H^{\ddagger}$ (kJ mol^{-1})	$\Delta S^{\ddagger}$ (J K^{-1} mol^{-1})	$\Delta V^{\ddagger}$ (cm^3 mol^{-1})	Mechanism	Ref.
$[Be(H_2O)_4]^{2+}$	7.3×10^5	59.2	+8.4	−13.6	A	[64]
$[Mg(H_2O)_6]^{2+}$	6.7×10^5	49.1	+31.1	6.7	I_d, D	[75]

activation volume. The new limits for water exchange rate on In^{3+} established by using Tb^{3+} as paramagnetic shift reagent [93] are about three orders of magnitude higher than the previous estimates [94].

Kowall [93] modeled water exchange mechanisms on Al^{3+}, Ga^{3+}, and In^{3+} using ab initio calculations at the Hartree–Fock level. Similar to transition metal ions, clusters with one ion and seven water molecules were considered [39]. For all three ions transition states and intermediates have been obtained for a dissociative pathway with structures similar to those found by Rotzinger (Fig. 3c). The energies of the dissociative transition state are in excellent agreement with the activation enthalpies, $\Delta H^{\ddagger}$, measured for $[Al(H_2O)_6]^{3+}$ and for $[Ga(H_2O)_6]^{3+}$ (Table 4) [91,31] The energy difference, $\Delta E^{\ddagger}_{\dagger}$, between the calculated intermediate and its corresponding transition state is relatively large for Al^{3+} and Ga^{3+}, but smaller for In^{3+}. The computation of transition states for an associative exchange mechanism was only successful for In^{3+}. The structures of the transition state and the intermediate for $[In(H_2O)_7]^{3+}$ are the same as those for $[Ti(H_2O)_7]^{3+}$ [39]. Furthermore, the associative pathway requires a much lower activation energy ($\Delta E^{\ddagger} = +29.1$ kJ mol^{-1}) than the dissociative water exchange ($\Delta E^{\ddagger} = +75.2$ kJ mol^{-1}). The calculated activation energy of $+29.1$ kJ mol^{-1} is in good agreement with the limit ≤ 33.1 kJ mol^{-1} for $\Delta G^{\ddagger}_{298}$ obtained experimentally [93].

Positive activation volumes for water exchange were measured on Al^{3+} and Ga^{3+} by variable-pressure NMR experiments, and a dissociative mechanism, I_d, was assigned. Due to the relatively large energy differences between transition state and intermediate calculated for these clusters, a limiting D mechanism was recently proposed from the calculations [93]. The much lower energy pathway for an a activated mechanism for In^{3+} together with the presence of a stable seven-coordinate intermediate allowed the assignment of an A mechanism for H_2O exchange at $[In(H_2O)_6]^{3+}$. Activation volumes were estimated from the ab initio cluster calculations using the Connolly surface [55]. The van der Waals radius of oxygen was adjusted to reproduce the experimental $\Delta V^{\ddagger}$ for Al^{3+} and Ga^{3+}. The corresponding activation volume for an associative exchange process calculated for In^{3+} was -5.2 cm^3 mol^{-1}. The change in mechanism from dissociative (Al^{3+}, Ga^{3+}) to associative (Sc^{3+}, In^{3+}) has already been observed experimentally for organic solvent exchange reactions [20].

Swaddle used a More–O'Ferrall type diagram, scaled to the volume as a physical parameter, to visualize the interplay between bond-making and bond breaking in

Table 4
Selected properties of reactants/products, transition states, and intermediates

Species	Description	Symmetry	Calculated			Experimental		
			$\Delta E^{\ddagger}$ (kJ mol^{-1})	$\Delta E_{\dagger}^{\ddagger}$ (kJ mol^{-1})	$\Delta V_{c}^{\ddagger}$ or ΔV_{c} (cm^{-3} mol^{-1})	$\Delta H^{\ddagger}$ (kJ mol^{-1})	$\Delta S^{\ddagger}$ (J K^{-1} mol^{-1})	$\Delta V^{\ddagger}$ (cm^{-3} mol^{-1})
$[Al(OH_2)_6 \cdot OH_2]^{3+}$	Linear hydrogen bond	C_s	0.0					
$\{[Al(OH_2)_5 \cdots OH_2OH_2]^{3+}\}^{\ddagger}$	Dissociative transition state	C_s	+85.4	10.7	+5.6	84.7	+41.6	+5.7
$[Al(OH_2)_5 \cdot (OH_2)_2]^{3+}$	Pentacoordinated intermediate	C_{2v}	+74.7		+7.1			
$[Ga(OH_2)_6 \cdot OH_2]^{3+}$	Linear hydrogen bond	C_s	0.0					
$\{[Ga(OH_2)_5 \cdots OH_2OH_2]^{3+}\}^{\ddagger}$	Dissociative transition state	C_s	+69.1	14.5	+4.8	67.1	+30.1	+5.0
$[Ga(OH_2)_5 \cdot (OH_2)_2]^{3+}$	Pentacoordinated intermediate	C_{2v}	+54.6		+6.9			
$[Ga(OH_2)_5 \cdot (OH_2)_2]^{3+}$	Water adduct	C_{2v}	+17.2					
$[Ga(OH_2)_5 \cdot (OH_2)_2]^{3+}$	Water adduct	C_2	+10.3					

Table 4 (*Continued*)

Species	Description	Symmetry	Calculated			Experimental		
			$\Delta E^{\ddagger}$ (kJ mol^{-1})	$\Delta E_{\mathrm{I}}^{\ddagger}$ (kJ mol^{-1})	$\Delta V_{\mathrm{c}}^{\ddagger}$ or ΔV_{c} (cm^{-3} mol^{-1})	$\Delta H^{\ddagger}$ (kJ mol^{-1})	$\Delta S^{\ddagger}$ (J K^{-1} mol^{-1})	$\Delta V^{\ddagger}$ (cm^{-3} mol^{-1})
$[In(OH_2)_6 \cdot OH_2]^{3+}$	Linear hydrogen bond	C_s	0.0					
$\{[In(OH_2)_5 \cdots OH_2OH_2]^{3+}\}^{\ddagger}$	*Dissociative* transition state	C_s	+75.2	5.6	+4.4			
$[In(OH_2)_5 \cdot (OH_2)_2]^{3+}$	Pentacoordinated *intermediate*	C_{2v}	+69.6		+4.8			
$\{[In(OH_2)_6 \cdots OH_2]^{3+}\}^{\ddagger}$	Associative transition state	C_1	+29.1	9.4	−5.2			
$[In(OH_2)_7]^{3+}$	Heptacoordinated intermediate	C_2	+19.7		−7.1			

simple interchange processes (Fig. 14). Based on Swaddle's semi-empirical model for partial molar volumes of metal ions in solution, Merbach choose ± 13.5 cm^3 mol^{-1} as the limiting value for *A* and *D* mechanisms [12]. The only measurable volume is, however, the activation volume, that is the volume difference between the transition state and the reactant. If, as Swaddle supposes, all water exchange reactions had to be regarded as interchange mechanism, the transition state would lie on the dashed diagonal in Fig. 14a. In this view, *A* and *D* mechanisms are considered as the limiting cases for the interchange mechanistic continuum and are, therefore, following the edges of the square diagram. However, from Rotzinger's [39,40] and Kowall's [93] calculations intermediates with increased and decreased coordination numbers have been identified and a different view of the square diagram was defined [93]. For concerted mechanisms (*I*), the single transition state lies, as before, on the ΔV diagonal axes. However, for stepwise mechanisms, the intermediate is situated on the diagonal while the two transition states lie symmetrically off to the diagonal. The intermediates must not necessarily lie on the corner of the square, which means that the absolute value of the volume difference between intermediate and ground state can be significantly smaller than $|\pm 13.5|$ cm^3 mol^{-1}. From calculated structures, Kowall et al. [93] derived volume changes for the transition states, $\Delta V_c^{\ddagger}$, and for intermediates, ΔV_c. These values are then used to draw reaction trajectories into the square diagram (Fig. 14b). As one would expect, transition states are about half the way between the reactant and the intermediate.

4. Water exchange from the second coordination shell

Information on the second coordination shell of water molecules around cations is much poorer than that on the first shell [3]. Properties of solvent molecules in this coordination shell are often very similar to those of the bulk, making their investigation extremely difficult. The analysis of radial distribution functions, $g(r)$, at long r distances, is difficult and much less reliable. The main source of structural information comes from neutron scattering [95] and X-ray [96–99] diffraction experiments on aqueous solutions. For cations with strong second shell solvation, such as the trivalent Al^{3+}, Cr^{3+}, or Rh^{3+}, information can be obtained from far infrared spectroscopy [100]. Computer simulations performed in close relation to experimental studies can deliver more insight into the microscopical structure and dynamics of solvent molecules in the second coordination shell [101,102].

Ions having a kinetically inert first coordination shell, like Cr^{3+}, offer experimentally the best opportunity to study second sphere exchange. Bleuzen et al. [101] showed in a combined experimental ^{17}O-NMR relaxation and computer modeling study that strong hydrogen bonding, due to polarization of first coordination sphere water molecules, leads to a structurally and kinetically well-defined second shell. From radial pair distribution functions, obtained from MD simulations on $Cr(ClO_4)_3$ in 277 H_2O molecules, peaks at 3.99 Å for oxygen and at 4.66 Å for hydrogen corresponding to the second coordination sphere are clearly distinguish-

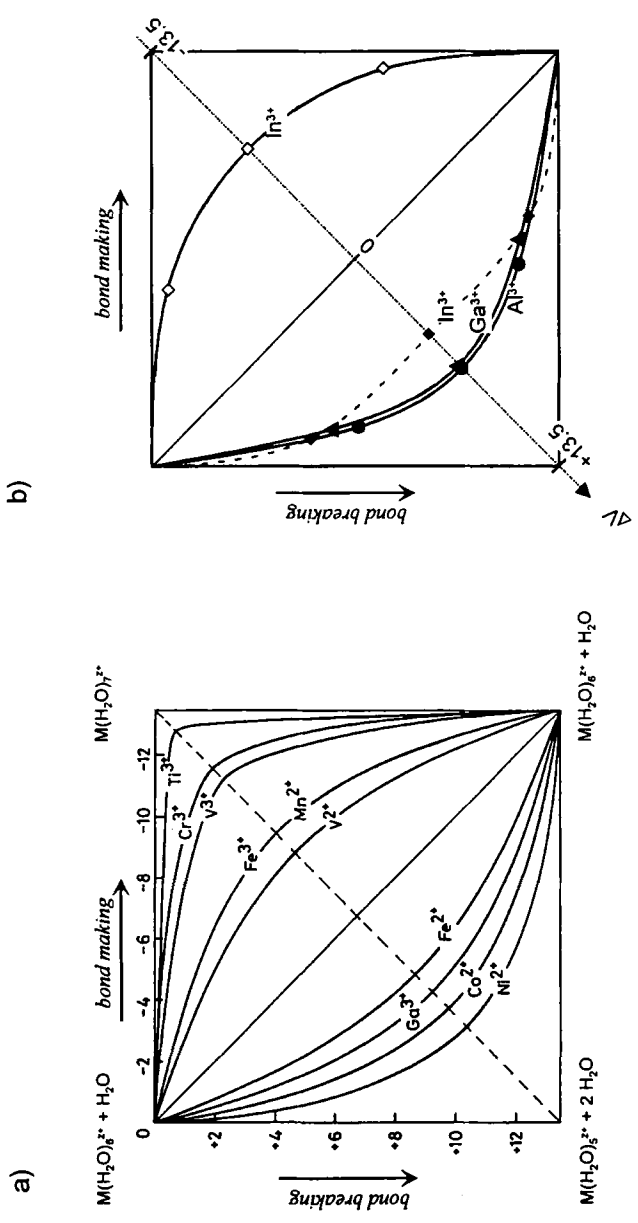

Fig. 14. Interpretation of activation volumes for water exchange on aqueous $[M(H_2O)_6]^{z+}$ in terms of contributions from bond making and bond breaking: (a) summary of volumes of activation for metal aqua ions, (b) calculated curves for Al(III), Ga(III), and In(III) using Connolly volumes.

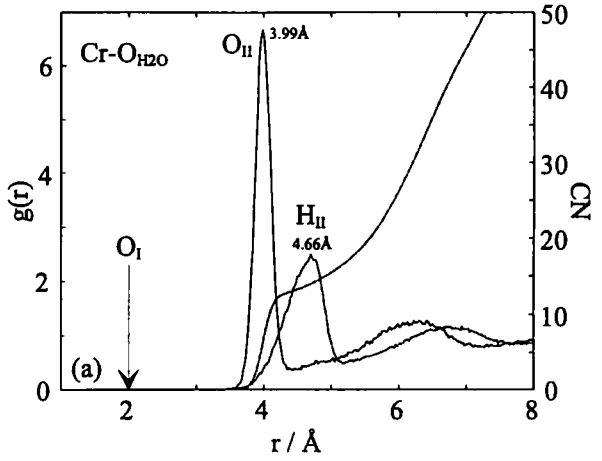

Fig. 15. Radial distribution function, $g(r)$, and running coordination number, CN, for the simulation of $[Cr(H_2O)_6]^{3+}$ in water. O_I shows distance of first shell water oxygens.

able (Fig. 15). Integration of the oxygen $g(r)$ between 3.00 Å and the first minimum at 4.45 Å gives the mean number of 12.9 water molecules for the second sphere of Cr^{3+} which agrees well with the values of 12–13.6 found experimentally [95,96]. The experimentally measured exchange rate constant of $k_{ex} = 7.8 \times 10^9$ s^{-1} (at 298 K) corresponds to a lifetime of 128 ps for one water molecule in the second coordination shell and is in good agreement with the lifetime of 144 ps observed from the molecular dynamics simulation. The angular distribution for the angle formed by the two exchanging water molecules shows a maximum at $\cos(\theta) \approx 0.76$, which represents an angle of about 40° (Fig. 16). The ion–oxygen distance vectors of two adjacent water molecules in the second coordination shell produces an angle of about 37°. Based on the simulation the following picture for an exchange

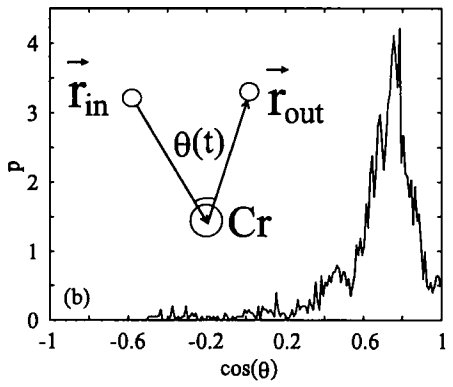

Fig. 16. Angular distribution for the angle formed by the entering water molecule, the Cr^{3+} ion, and the leaving water molecule around the moment of an exchange event.

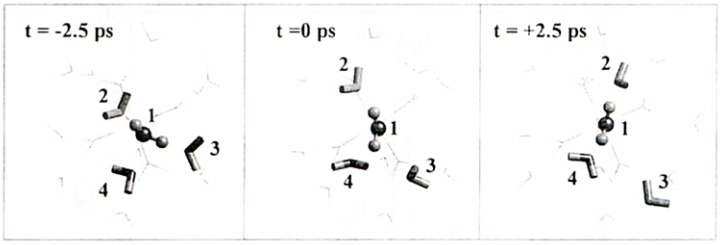

Fig. 17. Visualization of a water exchange between the second coordination shell and bulk solvent on $[Cr(H_2O)_6]^{3+}$ obtained from MD simulation: (1) selected first sphere water molecule; (2), (3) second sphere water molecules before exchange; (4) exchanging outersphere water molecule.

reaction between a second and a third sphere water molecule on $[Cr(H_2O)_6]^{3+}$ could be obtained (Fig. 17): In a first step a water molecule (no. 4 in Fig. 17) enters the second coordination sphere and increases the coordination number temporarily. In a second step the first sphere water molecule (no. 1), close to the entering one, rotates around its oxygen–chromium bond, then one of the hydrogen bonds formed to second sphere waters (no. 3 in Fig. 17) breaks up and a new hydrogen bond to the entering water molecule is formed. During the rotation the second hydrogen bond is maintained (no. 2 in Fig. 17). The third step consists of the leaving of the water molecule which has lost its hydrogen bond to the second sphere. This relatively simple picture agrees with the angle of about 40° degrees between the exchanging molecules resulting from the simulation (Fig. 16). The activation mode which can be attributed for this reaction from the MD simulation is associative.

Muñoz-Páez et al. [102] performed extended X-ray absorption fine structure studies on aqueous solutions of Cr^{3+} and Zn^{2+}. They detected second coordination shells in both cases with coordination numbers of 13.3 ± 1 (Cr^{3+}) and 11.6 ± 1.5 (Zn^{2+}). The same group performed Monte Carlo [103] and molecular dynamics [104] simulations of $[Cr(H_2O)_6]^{3+}$ in dilute aqueous solutions using an ab initio Cr^{3+} hydrate–water interaction potential. They found second shell coordination numbers of ~ 14 from both simulations. Furthermore, from simulations and EXAFS measurements they concluded that chloride ions are situated beyond the second hydration shell. Translational self-diffusion coefficients for second shell water molecules are much closer to those of the complex than to those of bulk water molecules. The authors conclude for this cation that the second hydration shell is joined tighter to the first shell than to the bulk water.

Near infrared experiments on lanthanide(III) ions showed no well defined second hydration shell [105]. MD simulations led to coordination numbers of water molecules in the second coordination sphere, CN_{II}, of 17.61 (Nd^{3+}, $CN_I = 8.98$), 17.13 (Sm^{3+}, $CN_I = 8.52$), and 16.74 (Yb^{3+}, $CN_I = 8.01$) (Fig. 8) [52]. The residence times for water molecules in the second shells around Nd, Sm and Yb are 13, 12 and 18 ps, respectively [56]. The slightly higher value for Yb^{3+} can be related to its smaller ionic radius, rion.

5. Concluding Remarks

The results reviewed in this paper clearly demonstrate that experimental studies and computer simulations or quantum chemical calculations are complementary. Due to the range of more than 18 orders of magnitude for water exchange rate constants on metal ions a variety of experimental techniques, mainly nuclear magnetic resonance, have to be applied. In a similar way, different computer techniques have to be used to calculate these simple chemical reactions in solution. Very fast exchange reactions like those on lanthanide ions or on second coordination shell can be simulated by classical molecular dynamics technique. Reaction pathways for water exchange on transition metal ions and on less labile first coordination shells can be followed by calculating clearly defined transition states and intermediates. Obviously, both techniques suffer from shortcomings: approximations on interaction potentials, missing of outer coordination shells. Nevertheless, they offer useful information that help the experimentalist understand underlying microscopic details of macroscopic observations.

Acknowledgements

The authors gratefully acknowledge financial support from the Swiss National Science Foundation and the Swiss Office for Education and Science (COST Program). Furthermore, we wish to thank the large number of people who have contributed to the work performed in Lausanne.

References

[1] D.T. Richens, The Chemistry of Aqua Ions, Wiley, Chichester, 1997.
[2] A. Cusanelli, U. Frey, D.T. Richens, A.E. Merbach, J. Am. Chem. Soc. 118 (1996) 6265.
[3] H. Ohtaki, T. Radnai, Chem. Rev. 93 (1993) 1157.
[4] P. Smirnov, H. Wakita, T. Yamaguchi, J. Phys. Chem. B 102 (1998) 4802.
[5] A.E. Merbach, J.W. Akitt, NMR Basic Princ. Prog. 24 (1990) 189.
[6] U. Frey, A.E. Merbach, in: J.-J. Delpuech (Ed.), Dynamics of Solutions and Fluid Mixtures by NMR, Wiley, Chichester, 1995.
[7] M. Eigen, Pure Appl. Chem. 6 (1963) 97.
[8] R. Car, M. Parrinello, Phys. Rev. Lett. 55 (1985) 2471.
[9] P. Caravan, A.E. Merbach Chem. Commun. (1997) 2147.
[10] C.H. Langford, H.B. Gray, Ligand Substitution Processes, Benjamin, New York, 1965.
[11] A.E. Merbach, Pure Appl. Chem. 54 (1982) 1479.
[12] A.E. Merbach, Pure Appl. Chem. 59 (1987) 161.
[13] T.W. Swaddle, Commun. Inorg. Chem. 12 (1991) 237.
[14] R.E. Connick, B.J. Alder, J. Phys. Chem. 87 (1983) 2764.
[15] R. van Eldik, Inorganic High Pressure Chemistry: Kinetics and Mechanisms, Elsevier, Amsterdam, 1986.
[16] R. van Eldik, Pure Appl. Chem. 64 (1992) 1439.
[17] R. van Eldik, A.E. Merbach, Commun. Inorg. Chem. 12 (1992) 341.
[18] T.W. Swaddle, M.K.S. Mak, Can. J. Chem. 61 (1983) 473.

[19] T.W. Swaddle, Adv. Inorg. Bioinorg. Mech. 2 (1983) 95.
[20] S.F. Lincoln, A.E. Merbach, Adv. Inorg. Chem. 42 (1995) 1.
[21] F.K. Meyer, K.E. Newman, A.E. Merbach, J. Am. Chem. Soc. 101 (1979) 5588.
[22] B.M. Rode, G.J. Reibnegger, S. Fujiwara, J. Chem. Soc. Faraday Trans. 2 (1980) 1268.
[23] D.H. Powell, L. Helm, A.E. Merbach, J. Chem. Phys. 95 (1991) 9258.
[24] Y. Ducommun, D. Zbinden, A.E. Merbach, Helv. Chim. Acta 65 (1982) 1385.
[25] Y. Ducommun, K.E. Newman, A.E. Merbach, Inorg. Chem. 19 (1980) 3696.
[26] A.D. Hugi, L. Helm, A.E. Merbach, Inorg. Chem. 26 (1987) 1763.
[27] A.D. Hugi, L. Helm, A.E. Merbach, Helv. Chim. Acta 68 (1985) 508.
[28] F.-C. Xu, H.R. Krouse, T.W. Swaddle, Inorg. Chem. 24 (1985) 267.
[29] T.W. Swaddle, A.E. Merbach, Inorg. Chem. 20 (1981) 4212.
[30] M. Grant, R.B. Jordan, Inorg. Chem. 20 (1985) 55.
[31] D. Hugi-Cleary, L. Helm, A.E. Merbach, J. Am. Chem. Soc. 109 (1987) 4444.
[32] I. Rapaport, L. Helm, A.E. Merbach, P. Bernhard, P. Ludi, Inorg. Chem. 27 (1988) 873.
[33] N. Aebischer, G. Laurenczy, A. Ludi, A.E. Merbach, Inorg. Chem. 32 (1993) 2810.
[34] G. Laurenczy, I. Rapaport, D. Zbinden, A.E. Merbach, Magn. Reson. Chem. 29 (1991) 45.
[35] R.J. Cross, Adv. Inorg. Chem. 34 (1989) 219.
[36] L. Helm, L.I. Elding, A.E. Merbach, Helv. Chim. Acta 67 (1984) 1453.
[37] L. Helm, L.I. Elding, A.E. Merbach, Inorg. Chem. 24 (1985) 1718.
[38] R. Åkesson, L.G.M. Pettersson, M. Sandström, U. Wahlgren, J. Am. Chem. Soc. 116 (1994) 8705.
[39] F.P. Rotzinger, J. Am. Chem. Soc. 118 (1996) 6760.
[40] F.P. Rotzinger, J. Am. Chem. Soc. 119 (1997) 5230.
[41] F.P. Rotzinger, Chimia 51 (1997) 97.
[42] M. Hartmann, T. Clark, R. van Eldik, J. Am. Chem. Soc. 119 (1997) 7843.
[43] R.J. Deeth, L.I. Elding, Inorg. Chem. 35 (1996) 5019.
[44] C. Cossy, A.C. Barnes, J.E. Enderby, A.E. Merbach, J. Chem. Phys. 90 (1989) 3254.
[45] C. Cossy, L. Helm, D.H. Powell, A.E. Merbach, N. J. Chem. 19 (1995) 27.
[46] A. Habenschuss, F.H. Spedding, J. Chem. Phys. 70 (1979) 2797.
[47] A. Habenschuss, F.H. Spedding, J. Chem. Phys. 70 (1979) 3758.
[48] A. Habenschuss, F.H. Spedding, J. Chem. Phys. 73 (1980) 442.
[49] T. Yamaguchi, M. Nomoura, H. Wakita, H. Ohtaki, J. Chem. Phys. 89 (1988) 5153.
[50] A.F.H. Spedding, L.E. Shiers, M.A. Brown, J.L. Derer, D.L. Swanson, A. Habenschuss, J. Chem. Eng. Data 20 (1975) 81.
[51] K. Miyakawa, Y. Kaizu, H. Kobayashi, J. Chem. Soc. Faraday Trans. 1 (1988) 1517.
[52] T. Kowall, F. Foglia, L. Helm, A.E. Merbach, J. Am. Chem. Soc. 117 (1995) 3790.
[53] T. Kowall, F. Foglia, L. Helm, A.E. Merbach, J. Phys. Chem. 99 (1995) 13078.
[54] C. Cossy, A.E. Merbach, Pure Appl. Chem. 60 (1988) 1785, and Refs. therein.
[55] M.L. Connolly, Science 221 (1983) 709.
[56] Th. Kowall, F. Foglia, L. Helm, A.E. Merbach, Eur. Chem. J. 2 (1996) 285.
[57] G. Laurenczy, A.E. Merbach, Helv. Chim. Acta 71 (1988) 1971.
[58] C. Cossy, L. Helm, A.E. Merbach, Inorg. Chem. 27 (1988) 1973.
[59] C. Cossy, L. Helm, A.E. Merbach, Inorg. Chem. 28 (1989) 2699.
[60] D.H. Powell, A.E. Merbach, Magn. Reson. Chem. 32 (1994) 739.
[61] D.P. Fay, D. Litchinsky, N. Purdie, J. Phys. Chem. 73 (1969) 544.
[62] P.S. Salmon, J. Phys. C: Solid State Phys. 20 (1987) 1573.
[63] P.S. Salmon, W.S. Howells, R. Mills, J. Phys. C: Solid State Phys. 20 (1987) 5727.
[64] P.S. Salmon, P.B. Lond, Phys. B 182 (1992) 421.
[65] P.-A. Pittet, G. Elbaze, L. Helm, A.E. Merbach, Inorg. Chem. 29 (1990) 1936.
[66] M. Alei, J.A. Jackson, J. Chem. Phys. 41 (1964) 3402.
[67] J. Frahm, H.-H. Füldner, Ber. Bunsenges. Phys. Chem. 84 (1980) 173.
[68] T. Yamagushi, H. Ohtaki, E. Spohr, E. Pálinkás, K. Heinzinger, M.M. Probst, Z. Naturforsch. A 41A (1986) 1175.
[69] D. Marx, M. Sprik, M. Parinello, Chem. Phys. Lett. 273 (1997) 360.
[70] N. Matwiyoff, H. Taube, J. Am. Chem. Soc. 90 (1968) 2796.

[71] A. Fratiello, R.R. Lee, V.M. Nishida, R.E. Schuster, J. Chem. Phys. 48 (1968) 3705.
[72] J. Jorgin, P.S. Knapp, W.L. Flint, G. Highberger, E.R. Malinowsky, J. Chem. Phys. 54 (1971) 178.
[73] W. Bol, G. Gerrito, C. von Panthaleon van Eck, J. Appl. Crystallogr. 3 (1970) 486.
[74] R. Caminiti, G. Licheri, G. Piccaluga, G. Pinna, J. Appl. Crystallogr. 12 (1979) 34.
[75] R. Caminiti, G. Cerioni, G. Crisponi, P. Cucca, Z. Naturforsch. A 43A (1988) 317.
[76] A. Bleuzen, P.-A. Pittet, L. Helm, A.E. Merbach, Magn. Reson. Chem. 35 (1997) 765.
[77] R.D. Shannon, Acta Crystallogr. Sect A 32 (1976) 751.
[78] M. Eigen, K. Tamm, Z. Elektrochem. 66 (1962) 107.
[79] J.K. Beattie, S.P. Best, B.W. Skelton, A.H. White, J. Chem. Soc. Dalton (1981) 2105.
[80] W. Bol, T. Welzen, Chem. Phys. Lett. 49 (1977) 189.
[81] R. Caminiti, G. Licheri, G. Piccaluga, G. Pinna, T. Radnai, J. Chem. Phys. 71 (1979) 2473.
[82] R. Caminiti, T. Radnai, Z. Naturforsch. 35A (1980) 1368.
[83] M. Maeda, H. Ohtaki, Bull. Chem. Soc. Jpn. 50 (1977) 1893.
[84] R. Caminiti, G. Paschina, Chem. Phys. Lett. 82 (1981) 487.
[85] A. Fratiello, R.E. Lee, V.M. Nishida, R.E. Schuster, J. Chem. Phys. 48 (1968) 3705.
[86] R.E. Connick, D.N. Fiat, J. Chem. Phys. 39 (1963) 1349.
[87] M. Alei, J.A. Jackson, J. Chem. Phys. 41 (1964) 3402.
[88] T.J. Swift, O.G. Fritz, F.A. Stephenson, J. Chem. Phys. 46 (1967) 406.
[89] D. Fiat, R.E. Connick, J. Am. Chem. Soc. 88 (1966) 4754.
[90] A. Fratiello, R.E. Lee, R.E. Schuster, Inorg. Chem. 9 (1970) 82.
[91] D. Hugi-Cleary, L. Helm, A.E. Merbach, Helv. Chim. Acta 68 (1985) 545.
[92] D. Fiat, R.E. Connick, J. Am. Chem. Soc. 90 (1968) 608.
[93] Th. Kowall, P. Caravan, H. Bourgeois, L. Helm, F.P. Rotzinger, A.E. Merbach, J. Am. Chem. Soc. 120 (1998) 6569.
[94] G.E. Glass, W.B. Schwabacher, R.S. Tobias, Inorg. Chem. 7 (1968) 2471.
[95] R.D. Broadbent, G.W. Neilson, M. Sandström, J. Phys. Condens. Matter 4 (1992) 639.
[96] M.C. Read, M. Sandström, Acta Chem. Scand. 46 (1992) 1177.
[97] R. Caminiti, G. Licheri, G. Piccagula, G. Pinna, J. Chem. Phys. 69 (1978) 1.
[98] W. Bol, T. Welzen, Chem. Phys. Lett. 49 (1977) 189.
[99] M. Magini, J. Chem. Phys. 73 (1980) 2499.
[100] P.-A. Bergström, J. Lindgren, M.C. Read, M. Sandström, J. Phys. Chem. 95 (1991) 7650.
[101] A. Bleuzen, F. Foglia, E. Furet, L. Helm, A.E. Merbach, J. Weber, J. Am. Chem. Soc. 118 (1996) 12777.
[102] A. Muñoz-Páez, R.R. Pappalardo, E. Sánchez Marcos, J. Am. Chem. Soc. 117 (1995) 11710.
[103] R.R. Pappalardo, J.M. Martínez, E. Sánchez Marcos, J. Phys. Chem. 100 (1996) 11748.
[104] J.M. Martínez, R.R. Pappalardo, E. Sánchez Marcos, K. Refson, S. Díaz-Moreno, A. Muñoz-Páez, J. Phys. Chem. B 102 (1998) 3272.
[105] P.-A. Bergström, J. Lindgren, Inorg. Chem. 31 (1992) 1529.